Experimental study on the effect of soil moisture content on critical temperature rise for typical cable backfill materials

Karlis Rieksts, Espen Eberg

***Abstract*—The increased utilization of power grid requires operating power cables close to their thermal limit. Buried power cables in such condition experience thermal instability where thermal resistance increases as the moisture migrates away from the proximity of the cable forming a dry-out zone. While it is common to use a two-zone model to account for the dry-out zone in ampacity calculations, there is a limited number of studies on characterizing backfill materials for their critical temperature rise ($\Delta\theta_x$), especially for crushed rock sands. In addition, dependency of the $\Delta\theta_x$ on moisture content is sometimes not acknowledged. This study measures the $\Delta\theta_x$ for three typical backfill materials and investigates the relationship between $\Delta\theta_x$ and moisture content. The results show that crushed rock sand has higher $\Delta\theta_x$ compared to natural sand. Overall, large range of $\Delta\theta_x$ was measured depending on moisture content and type of soil. Ampacity calculations with the established $\Delta\theta_x$ show that at low moisture content, the thermal resistivity of the soil has a higher influence on ampacity than $\Delta\theta_x$. At relatively high moisture content, the $\Delta\theta_x$ becomes the predominant factor governing the overall ampacity.**

I. INTRODUCTION

ELECTRIFICATION of society and increased production of renewable power demands increased utilization of the power grid. Electric power cables must then be operated close to their thermal limit, where risk of failure is minimized and expected lifetime sustained. When cables are operated at high temperatures, up to 90°C conductor temperature for XLPE insulated cables, there will be a large temperature gradient in the surrounding soil, which can lead to drying of the soil in vicinity of the cable due to moisture migration from hot to cold regions [1], [2].

The thermal resistivity of soil is strongly dependent on the moisture content in the soil [3]–[6], where dry soils can have up to three times the thermal resistivity of a moist soil. de Leon and Anders [7] found that the external thermal resistance of the cable accounts for up to 70% of the temperature increase in the cable, hence the drying the of soil in vicinity of the cable will have great impact on the resulting ampacity. The dry out zone can have a substantial impact on the overall ampacity. Gouda et al. reports derating factors down to 0.872 for natural soils [8], and down to 0.86 for artificial soils with increased content of lime [9] which corresponds to 13% and 14% reduction in ampacity if dry zone is considered, respectively. In areas, where the moisture content (percent of soil dry weight, symbol *w*) can be below 5%, the dependency of thermal properties of the soil on moisture is thus crucial [10].

The most common method for estimating ampacity of buried power cables is by using the formulae of the IEC 60287 standard [11], [12]. To account for dry-out zone around cable and the resulting increase in thermal resistivity, a modified version have been implemented in the IEC standard [2]. The modified equation introduces the variables of cable temperature rise ($\Delta\theta$) and critical temperature rise of soil ($\Delta\theta_x$) above ambient temperature (θ_a).

A hydrologically stable condition is defined as one where the outflow of water vapor driven by temperature gradient is balanced by the inflow of water through the process of capillarity driven by the moisture gradient [13]. When characterizing thermal instability of different soils, it has been common to refer to the critical moisture content or sometime the critical degree of saturation (volume of water to volume of voids in soil, defined in (5) in Appendix A, symbol S_r) [13]–[17]. Under the critical moisture content, the vapor outflow is in disbalance with the inflow of liquid flow. This results in a net loss of moisture that is adjacent to the power cable [16]. The critical moisture content is also typically referred to the moisture content where the water phase through the soil matrix becomes discontinued and has a large effect on thermal resistivity. Below the critical moisture content, further small decrease of moisture results in a disproportionate increase in thermal resistivity of the soil. The critical moisture content generally decreases with improved particle size distributions (well graded) and the level of compaction [16]. Reference [17] defines the critical degree of saturation to the value of thermal resistivity that is 10% higher than the asymptotic value. While the moisture content has a strong non-linear relationship with the soil thermal resistivity, the effect of it on the $\Delta\theta_x$ is not entirely characterized. Hence this study investigates determination of $\Delta\theta_x$ for different soil types and more importantly the relationship between moisture content and $\Delta\theta_x$.

There is a limited amount of experimentally determined values of $\Delta\theta_x$. The experiments vary with their soil composition, configurations, boundary conditions and soil moisture contents [8], [9], [18], [19]. Some studies have focused on the determination of critical moisture content [13], [14], [16]. Multiple studies have developed numerical models for moisture migration around power cables [7], [18], [20], [21]. However, although these models validate aspects of moisture migration around power cables, they do not provide $\Delta\theta_x$ that could be used when calculating ampacity.

In this work the drying of three different soils, one natural soil and two thermal backfills made from crushed rock (often referred to as "stone dust" [10]) and all commonly used as thermal backfills in Norway/Europe, were characterized in a scaled cylindrical test rig. The study first and foremost

measured $\Delta\theta_x$ for different moisture contents. In addition, multiple geotechnical tests were carried out to characterize the soils to determine the parameters that have the largest impact on the $\Delta\theta_x$. The experimental results were also compared to the method by CIGRE for determining the critical temperature [17], in order to evaluate how representative this method is for commonly used soils. The study also evaluated the effect of experimentally determined $\Delta\theta_x$ on the ampacity values.

II. Materials

Three thermal backfill materials with particle size 0-4 mm were selected for testing, which all are commonly used for buried cable installations in Norway. The materials vary with their mineral composition, particle size distribution and the amount of fines content. First material was a washed crushed rock sand (REN) with controlled amount of fines of about 6%. Although the material has a low fines content, the material is relatively fine graded, with a large content of particles in the range from 63 to 250 µm. About 18% of the material was finer than 125 µm and 30% of material was finer than 250 µm. The second material was a natural sand (NAT) with a typical uniformly graded particles size distribution and fines content around 3.5%. The third material was an unwashed crushed rock sand (VAS) with fines content around 10%. Table I gives a summary with material particle/mineral density (ρ_s) [22], particle/mineral thermal conductivity (k_s) measured using the method described in Section III.B, and maximum dry density ($\rho_{d\ max}$). Fig. 1 shows the range of particle size distribution [23] for the three tested materials. The solid line refers to the mean value, while the shaded areas correspond to the range of variation.

TABLE I
Material Characteristics

Material	Tag	ρ_s, g/cm^3	k_s, W/mK	$\rho_{d\ max}$, g/cm^3
Crushed rock	REN	2.962	2.5	2.18
Natural sand	NAT	2.740	5.0	1.95
Crushed rock	VAS	3.069	2.5	2.42

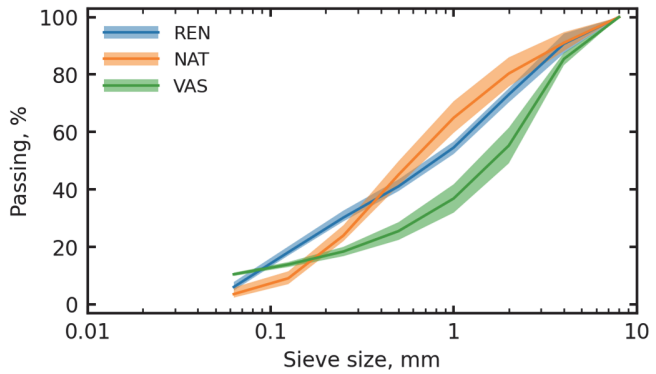

Fig. 1. The range of particle size distribution for tested materials.

Fig. 2 shows the proctor density [24] for the three tested materials. The grey lines correspond to the saturation values for each of the materials. The results show that the maximum dry density at the optimum moisture content (w_{opt}) was 2.18 g/cm^3 for REN (w_{opt}=8%), 1.95 g/cm^3 for NAT (w_{opt}=10%) and 2.42 g/cm^3 for VAS (w_{opt}=8%).

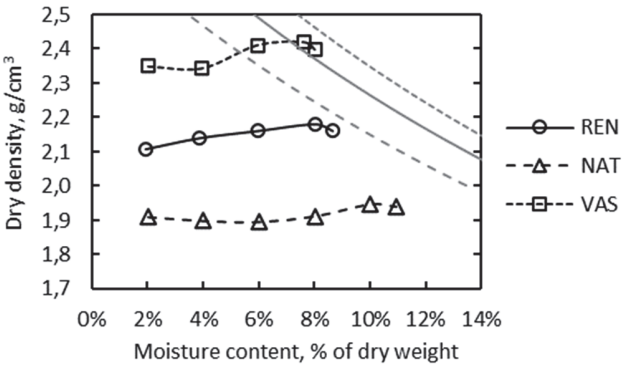

Fig. 2. Maximum compaction and optimum moisture content.

Recommended practice for backfill materials in Norway is using a material with specification 0-4 mm particle size (2% up to 8 mm) and less than 7% of fines (<0.63 µm). All materials exceed the requirement for particles above 4 mm having around 10% in the 4-8 mm range. For the fines content, the REN and NAT materials fulfil the requirements, but the VAS material has to large amount of fines. The VAS material is more representative to common buried cable installations, as this currently is the most available material.

III. Experimental Procedure

Fig. 3 shows the flowchart of experimental procedure to characterize and test materials for their dry-out conditions. To fulfil the goal, the experimental procedure was divided into three parts: i) general characterization; ii) special characterization; iii) closed-system radial heating test. The general characteristics gives the basic geotechnical properties, e.g., maximum compaction density, optimum moisture content, particle density. Special characterization involves more detailed tests regarding the soil thermal and hydraulic properties. These are properties that more directly govern the dry-out process. The last part is the main experiment to test materials for their dry-out response under various moisture and power conditions.

For all tests only a slight compaction was applied. This corresponds to typical cable installation process when only a limited compaction is used. To account for the effect of moisture variation on the critical temperature rise ($\Delta\theta_x$), the radial heating test was carried out with 1.6%, 2.4% and 3.2% of water. The other characterizing tests were carried out with the same moisture contents of 1.6%, 2.4% and 3.2% and compaction levels as used in the radial heat test within an accuracy of 5%.

A. Water retention

Water retention under uniform temperature conditions for a prolong period was determined using a simple test method. The samples were compacted in a 19 cm high and 12.5 cm diameter container and sealed at the top to prevent water evaporation. The three test materials were prepared with 1.6%, 2.4% and 3.2% moisture content. The top of the sample was sealed to prevent from evaporation. After a 9-day period, each sample was taken out from the container in 10 layers and water content was determined for each of the layer. The results allow to determine the moisture content that can be held by the material under isothermal temperature conditions.

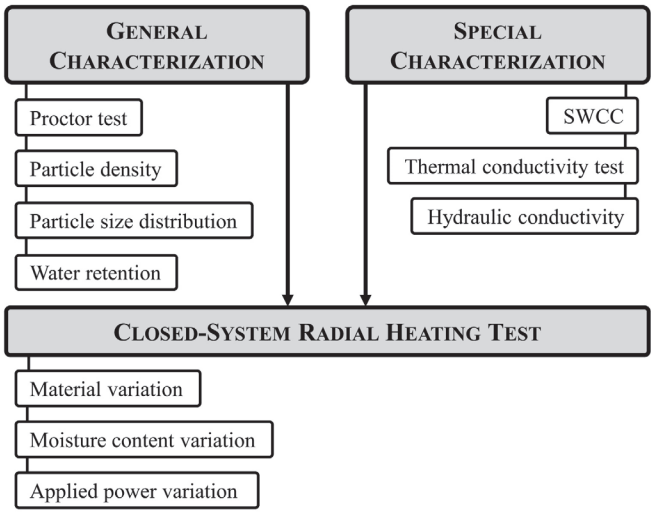

Fig. 3. Flow chart of laboratory tests to characterize dry-out phenomena of cable sand.

B. Thermal conductivity test

Thermal conductivity tests were carried out to confirm the modelled values of thermal dry-out curves. Thermal conductivity was tested for selected moisture contents 1.6%, 2.4% and 3.2%. A steady-state test method was used to measure thermal conductivity [5], [25], with test apparatus as outlined in Fig. 4. The soil was compacted in a PVC mold with a height and inner diameter of 75 and 100 mm, respectively. The sample was placed between borosilicate glass discs. The glass discs have known thermal conductivity and combined with temperature measurement on both sides of the discs the heat flux is calculated. The three-layer system was sandwiched between two independent heat exchange plates which allowed to control the vertical temperature gradient. To maintain a one-directional heat flow and reduce a radial heat loss, the sample was insulated with 10 cm of XPS insulation. The temperature was set to 7°C at the top and 3°C at the bottom, and the setup was placed in a cabinet with ambient temperature of 5°C. The thermal conductivity for a given sample based on the steady-state measurements is given by

$$\lambda = \frac{Q_{uf}+Q_{lf}}{2} \cdot \frac{h_s}{(T_T - T_B)} \quad (1)$$

where Q_{uf} and Q_{lf} are the heat flux values from the upper and lower heat flux sensor (W/m^2), h_s is the sample thickness (m) and T_T and T_B are the temperatures (°C) at the top and bottom of the soil sample, respectively.

Three samples were tested for each moisture content. To establish a full thermal dry-out curve, the thermal conductivity model proposed by [5], [26], and based on the study by [4] was used. Saturated samples with particle size 1-2 mm were tested to determine the particle/mineral thermal conductivity based on the geometric mean method [27], where (7) is solved for λ_s.

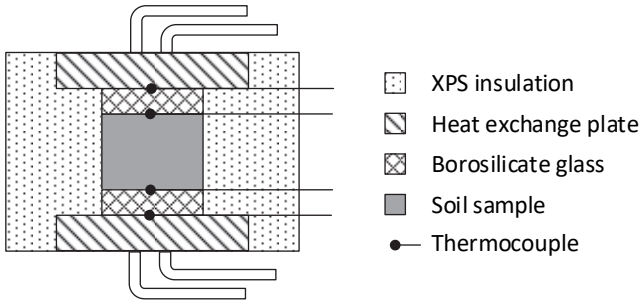

Fig. 4. Steady-state setup for measuring thermal conductivity/resistivity.

C. Hydraulic conductivity test

Hydraulic conductivity tests were carried out with a KSAT device using falling head technique [28]. The sample volume was 250 cm^3. The samples were lightly compacted to be consistent with the rest of the experiments. Due to the constrains of maximum particle size that can be used for the subsequent determination of soil-water characteristic curve, particles above 4 mm were removed. The 4+ mm particles account for about 10% of the material. To assess the effect of removing coarse particles on hydraulic conductivity and porosity, samples with and without the 4+ mm particles were tested. At least 5 samples were tested for each of the material.

D. Soil-water characteristic curve

The soil water characteristic curve was determined through evaporation experiment with the HYPROP (Hydraulic property analyser) device [29]. The method is based on evaporation experiment proposed by Wind [30] and later modified by Schindler [31]. Each sample was first tested for its hydraulic conductivity and subsequently the sample was mounted on two tensiometers to determine soil-water characteristics curve. The measurement from hydraulic conductivity was added to the measured dataset and the model by Fredlund et al. [32] was used to fit the experimental data. Three soil-water characteristic curve measurements were done for each of the material. The final fitted line is based on these three measurements.

E. Closed system radial heating test

The design of the closed system radial heating test was based on the experimental procedure used by [33], [34]. The test cell consisted of a horizontally placed cylindrical sample with longitudinal heating element in the centre and cooling control on the outside wall. The outer shell of the test setup was a stainless-steel tube with an inner diameter of 600 mm and wall thickness of 4 mm. A copper tube with diameter of 12 mm was wrapped around the outer wall as a double helix to provide a surface temperature constant with time and position. The average gap between each revolution was around 20 mm. The gaps between the copper tubes were filled with silicone paste mixed with aluminium powder. To minimize heat loss and to maintain a more uniform temperature, a layer of rock wool was wrapped around the outside. The copper tube circuit was attached to a cryostat for temperature control, providing an ambient temperature, θ_a, of 10 °C used for all tests in this work.

The centre heating element consisted of a stainless-steal core with a diameter of 60 mm (Fig. 5c). A heating wire with a total

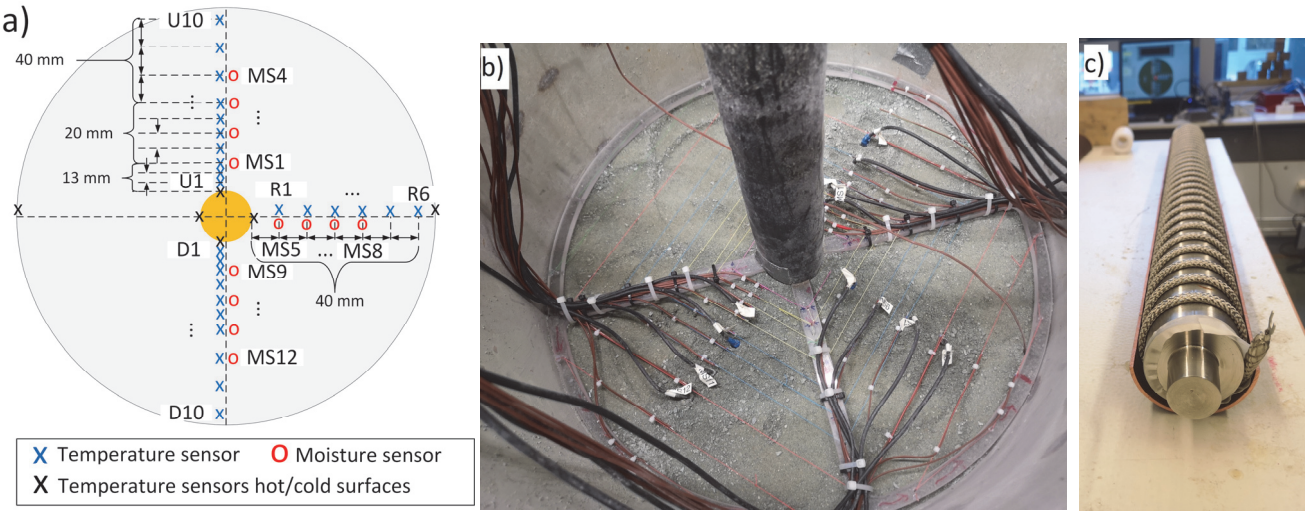

Fig. 5. a) temperature and moisture sensor location. Distances for sensors D1-D10 and MS9-MS12 are the same as for U1-U10 and MS1-M4, respectively; b) sensors placed in the middle part of a sample; c) heating cable wrapped around the steel core.

length of 6 m was wrapped around the core with 20 mm gap between each of the wire revolutions. To provide a uniform temperature distribution, a copper pipe split into four sections, was secured with clamps over the cable. The thickness of the copper pipe was 2 mm, and the outside final diameter of the heating element was 74 mm.

In total 32 thermocouples were used to measure temperature profile in different directions. Ten thermocouples were placed in upward (U1-10) and downward (D1-D10) direction, six were placed sidewards (R1-R6), four sensors were attached to the core and two sensors were placed on the wall, where average values are named hot and cold end, respectively. The sensor placements are shown in Fig. 5a, where the distances given are between neighbouring sensors, e.g. U1 and U2 are 13 mm apart and R1 and R2 are 40 mm apart. The physical implementation is shown in Fig. 4b.

Four *EC-5* moisture sensors were placed in upward (MS1-MS4), downward (MS9-MS12), and sideward (MS5-MS8) directions. The sensors were place 4, 8, 12 and 16 cm away from the heating element. As measured by Sakaki [35], the effective measurement distance is 1 cm perpendicular to the probes. The distance between each sensor was thus sufficiently large to avoid disturbance from one another. The moisture sensors are temperature dependent and precise measurements at low moisture content is difficult to achieve. Multiple studies have addressed these issues [35]–[37].

IV. Results

A. Water retention

Fig. 6 shows the results for water retention after 9-day period for materials with varying water content. For moisture content of 1.6% and 2.4% there is only a marginal accumulation of water at the bottom part of the sample. This shows that all materials with water content below 2.4% is below the critical degree of saturation. When tested with moisture content of 3.2% REN and NAT showed noticeable moisture gradient indicating that the moisture level is above the normal retention level. VAS material retained a well distributed moisture at this moisture level showing that moisture content of 3.2% is below the critical degree of saturation. These results are largely in line with moisture distribution in radial heat transfer experiments presented later.

B. Thermal conductivity test

Fig. 7 shows the modelled thermal dry-out curve, using the model by Côté and Konrad [5] as given in Appendix A, and measured values at different moisture contents, and values are tabulated in Table II. Each of the measured data points is an average of three measurements. The results show some deviation between modelled and measured values. However, this is expected as the accuracy of the thermal conductivity models is generally around 15-20% [5], [26]. Nevertheless, the

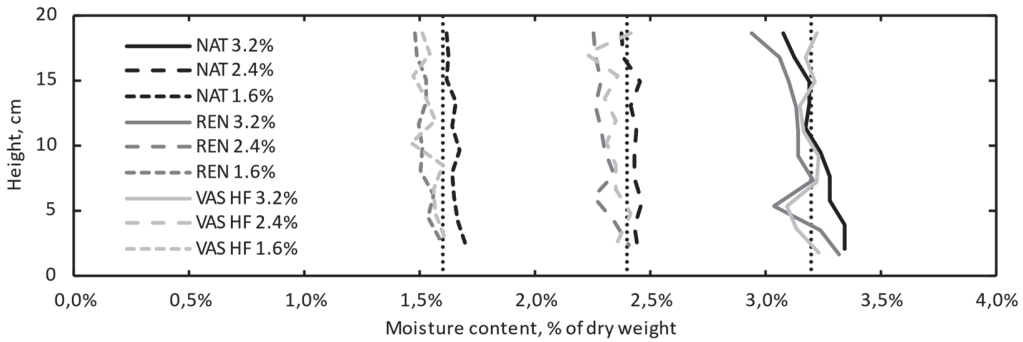

Fig 6. Water retention for three tested materials after 9 days with varying water content.

experimental results show that at the given moisture content from 1.6% to 3.2%, natural sand has a substantially lower thermal resistivity compared two crushed rock sand, with average value of 0.8 K.m/W compared to 1.0 K.m/W for REN and 1.1 K.m/W for VAS sands. It is also seen the REN sand is less sensitive to moisture content with 13% decrease from 3.2% to 1.6 % moisture content, while NAT and VAS has an increase of 21% and 18%, respectively. Fig. 7 also shows the critical degree of saturation that corresponds to the thermal resistivity value that is 10% higher that the asymptotic value [17]. Based on this evaluation, all values of moisture content are below the critical value. However, water retention test showed that NAT and REN material has free water at 3.2% moisture content.

TABLE II
MEASURED AND MODELLED THERMAL RESISTIVITY IN SOILS. W IS MOISTURE CONTENT AND TR IS THERMAL RESISTIVITY.

Mat-erial	S_r	w, % of dry weight	Measured TR (K.m/W)	Modelled TR (K.m/W)	ΔTR
REN	0,11	1,6	1,08	1,33	23 %
	0,16	2,4	1,05	1,15	10 %
	0,20	3,2	0,94	1,06	13 %
NAT	0,10	1,6	0,89	1,00	12 %
	0,15	2,4	0,76	0,86	13 %
	0,19	3,2	0,7	0,79	13 %
VAS	0,12	1,6	1,19	1,08	-9 %
	0,16	2,4	1,13	0,97	-14 %
	0,20	3,2	0,98	0,89	-9 %

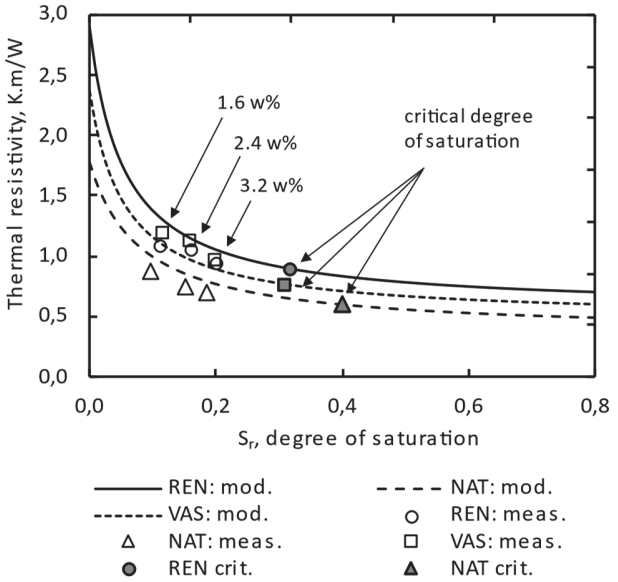

Fig.7. Modelled thermal dry-out curve and experimental measurements of thermal resistivity.

C. Hydraulic conductivity test

The hydraulic conductivity tests were carried out with and without particles that are larger than 4 mm. The reason for removing the course particles is the size limitation of material for soil-water characteristic test which is run with the same sample. Although the HYPROP test is suitable for sands the experience shows that particles larger than 4 mm are problematic when the tensiometer prongs are pushed into the sample. Fig. 8 shows the comparison between materials and the effect of removing particles larger than 4 mm while Fig. 9 shows the effect of 4+ mm particles on porosity. The results generally show that REN and VAS materials has significantly lower hydraulic conductivity compared to NAT while the porosity is roughly the same for all materials. This means that the pore size on average is smaller for REN and VAS and that should have a favourable effect on dry-out process.

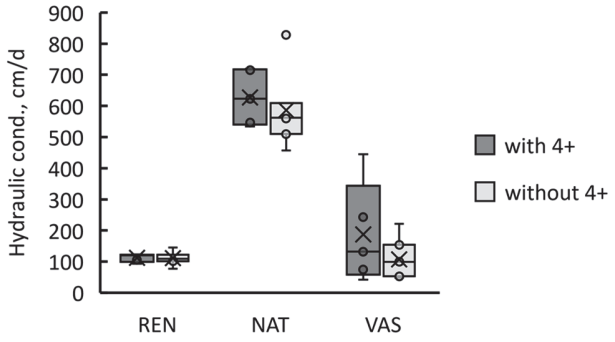

Fig. 8. Hydraulic conductivity.

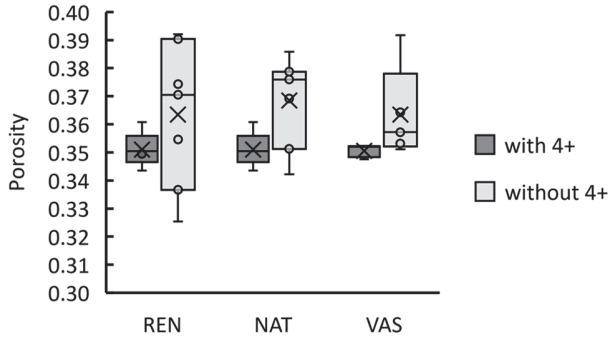

Fig. 9. Porosity changes without 4+ particles.

D. Soil-water characteristic curve

Fig. 10 shows the soil-water characteristic curve for the three materials. Each of the curves is a fitted line based on the experiments. For each material, three samples were tested, with general properties given in Table III, where n is porosity, ρ_d dry density and k is hydraulic conductivity. The results reveal that VAS material for a given suction value can hold higher amount of moisture. The two other materials show very similar results. Based on CIGRE [1] soil-water characteristic curve should provide some indication on the differences between critical temperature for different materials. In practice, materials that have higher moisture content for a given suction value should essentially have higher critical temperature. The superiority of VAS material to hold more water can mostly be explained by the amount of fines which is substantially higher than other materials. The soil-water characteristic curve for VAS material is in line with experimental observations for critical temperature. However, the soil-water characteristic curve fails to explain the large differences observed for REN and NAT materials. During heating tests, REN material showed significantly higher critical temperature. It could be that the soil-water characteristic curve does not fully capture the water retention capacity of REN material.

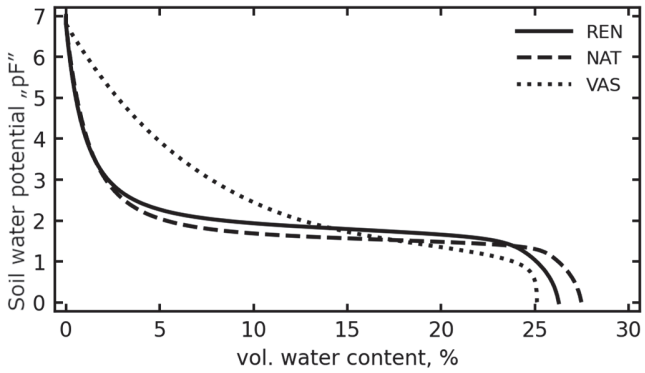

Fig. 10. Soil-water characteristic curve.

TABLE III
SAMPLE PROPERTIES FOR SOIL-WATER CHARACTERISTIC CURVE TEST

material	n	ρ_d, g/cm^3	k, cm/d
REN	0.37	1.90	101
	0.34	2.01	105
	0.33	2.04	110
NAT	0.39	1.68	510
	0.35	1.79	828
	0.36	1.77	457
VAS	0.39	1.87	48
	0.36	1.98	221
	0.35	2.01	99

E. Closed system radial heating test

In total 10 samples were tested with different moisture and applied power. Table IV summarizes all samples and their corresponding general properties and heating conditions, where $w\%_{prep}$ and $w\%_{fin}$ are prepared and final moisture content by dry weigh percent before and after test, respectively and $S_{a,prep}$ and $S_{a,fin}$ are prepared and final moisture saturation before and after test, respectively, P is applied heat power and Q the applied heat flux. The dry density for all the samples is significantly below their maximum values. REN was compacted on average at 89%, NAT at 90% and VAS at 80% of the maximum compaction. Given that all samples were compacted with approximately the same amount of power, the relatively large amount of fines and well-graded particle distribution of VAS is reflected in significantly lower compaction to the other two materials. The final water content show that some water has evaporated during the tests. However, the final water content is more than 95% of the initial water content.

Fig. 11 shows the REN sand at the end of the heating phase. A clear dry-out zone can be seen for all the samples, where it can be seen that the dry-out zone generally gets larger for smaller moisture content.

Fig. 12 and 13 shows moisture and temperature gradient at the end of the test. Since higher power was applied to samples with higher moisture content, also the measured maximum temperature increases with higher moisture content. This was done to be able to induce a dry-out zone for the higher moisture contents. The combination of low power (170 W) and high moisture content (3.2, %) did not give a dry-out zone. E.g., 170 W/m applied power to samples with 3.2% moisture content did not induce any dry-zone formation. These measurements are typically used for the determination of $\Delta\theta_x$ [8], [18]. However, with the given experimental results it was clear that determining accurate $\Delta\theta_x$ can be difficult due to multiple reasons. First, moisture profile plots are based on moisture measurements that are a volume average for each 4 cm of sample radial distance. Hence, getting precise location of the transition zone is not possible in this way. The transition zone can be more accurately determined from simple visual inspection as shown in Fig. 11. However, the size of the dry zone has some variation depending on the direction and evaporation after opening slightly altered the size of the visual zone.

Hence, using the determined location of dry zone to read temperature from temperature profile plot could introduce some inaccuracies. In some studies, only temperature profile has been used to determine the $\Delta\theta_x$ [8], [9]. However, as pointed out by Oh & Tinjum [18], temperature profile does not always have a clear change in the temperature gradients. One of the reasons, is the fact that transition between the two zones is very gradual as can be seen by the moisture profiles (Fig. 13). Another reason is that, if the core temperature was exceeding about 100 °C, the sample did not fully stabilize (see Fig. 15a). The reason for that can be twofold. First, the experimental setup is not a truly closed system and at high temperature creates enough pressure difference, so the moisture evaporates out of the system. Second, the test time was not sufficiently long to reach a steady state.

TABLE IV
SAMPLE PROPERTIES FOR RADIAL HEATING TEST, W% IS MOISTURE CONTENT

Material	tag	n	ρ_d	$w\%_{prep}$	$w\%_{fin}$	S_{a_prep}	S_{a_fin}	P, W	Q, W/m^2
Crushed rock (REN)	SN13	0.35	1.98	3.2%	2.99%	0.18	0.17	320	1529
	SN14	0.36	1.94	3.2%	3.15%	0.17	0.17	320	1529
	SN16	0.35	1.89	3.2%	3.10%	0.17	0.17	320	1529
	SN26	0.35	1.89	2.4%	2.32%	0.13	0.12	244	1166
	SN18	0.34	1.94	1.6%	1.53%	0.09	0.09	170	812
Natural sand (NAT)	SN15	0.37	1.71	3.2%	3.11%	0.15	0.14	320	1529
	SN27	0.37	1.73	2.4%	2.22%	0.11	0.10	220	1051
	SN6	0.33	1.84	1.6%	1.53%	0.09	0.09	170	812
Crushed rock (VAS)	SN25	0.39	1.87	3.2%	2.98%	0.15	0.12	320	1529
	SN9	0.34	2.01	1.6%	1.54%	0.09	0.09	170	812

Given that steady state measurements could lead to inaccurate determination of $\Delta\theta_x$, time series data were further investigated for this use. Generally, temperature sensor data can provide the indication of the progression of the dry zone. In simple terms as the dry zone passes by a temperature sensor there is a rapid temperature increase due to increasing thermal resistivity. Fig. 14 shows the time series for four moisture sensors along with the corresponding temperature sensors at the same locations. The values for moisture sensors were normalized for a better visual representation. Following the trend of both measurement lines for a specific location gives an insight on the progression of the formation of the dry zone. The progression can be split into four distinctive phases. During the first phase there is a steep increase in the moisture measurement values which is solely attributed to the temperature dependency of the sensor.

The first phase (P1) is finished when the moisture sensor reaches its peak value. During the second phase (P2), despite the temperature dependency of the moisture sensor, the value

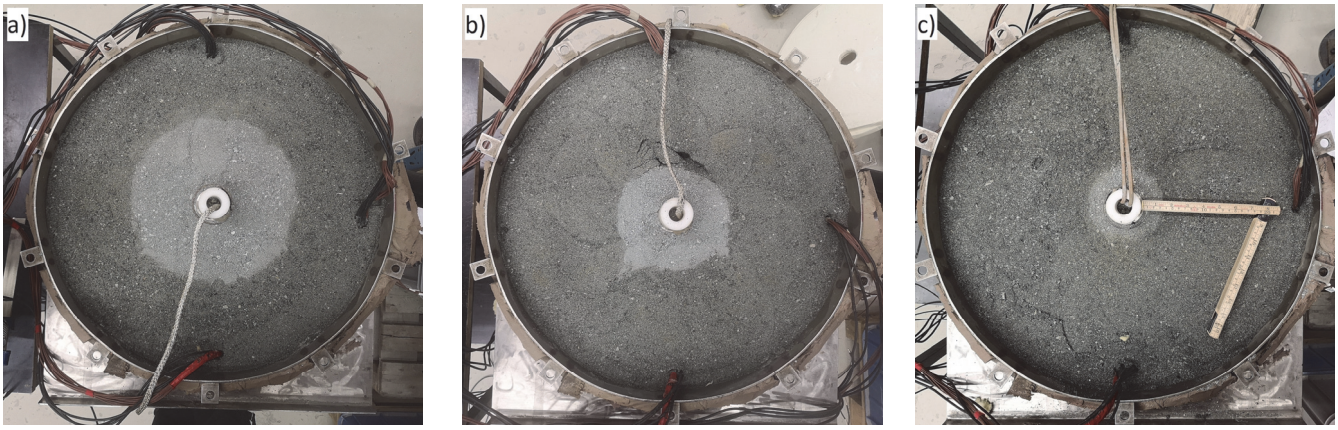

Fig. 11. Formation of dry zone under steady state conditions for REN material with different moisture content: a) 1.6% moisture; b) 2.4% moisture; c) 3.2% moisture.

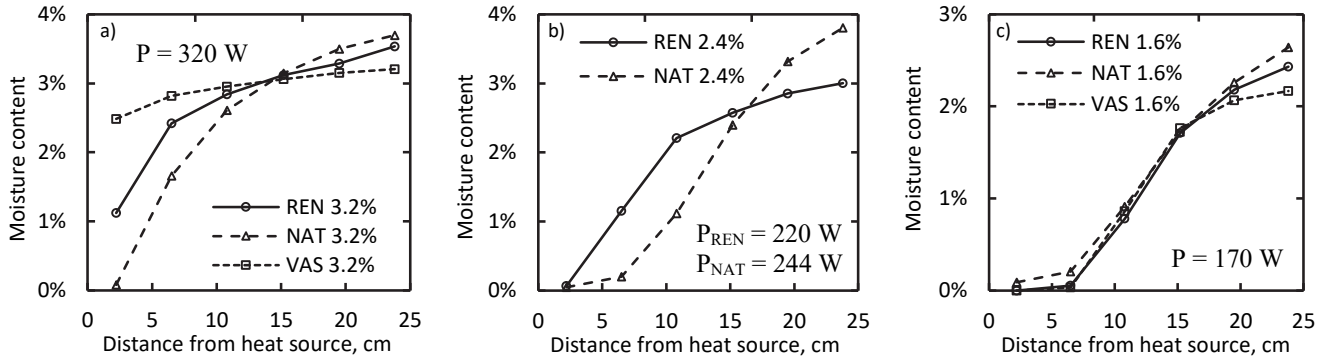

Fig. 12. Moisture profile after test for three tested cable sands with different amount of moisture content: a) moisture content of 3.2%; b) moisture content of 2.4%; c) moisture content of 1.6%.

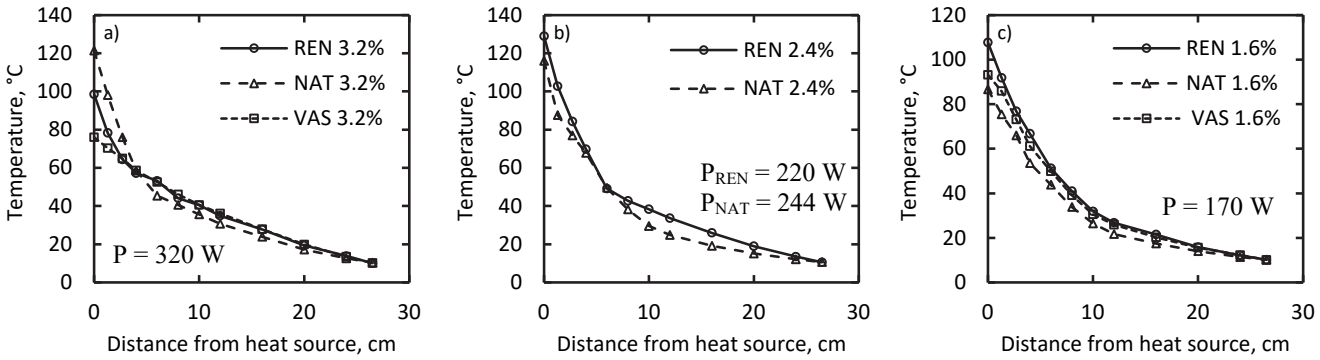

Fig. 13. Temperature profile after test for three tested cable sands with different amount of moisture content: a) moisture content of 3.2%; b) moisture content of 2.4%; c) moisture content of 1.6%.

This article has been accepted for publication in IEEE Transactions on Power Delivery. This is the author's version which has not been fully edited and content may change prior to final publication. Citation information: DOI 10.1109/TPWRD.2022.3220954

starts to decrease rapidly. The end of the second phase is reached when there is noticeable increase of temperature. This point in temperature readings is considered as the critical temperature. The reason why moisture sensor value is decreasing before any critical change in temperature is most likely because the moisture sensors are measuring a volume average. According to Sakaki [35], the EC-5 sensors measure about 1 cm away perpendicularly to the two prongs. This means that the moisture sensor starts to detect the approaching dry zone when the dry zone is about 1 cm away from the temperature sensor. The third phase (P3) continues after the moisture sensor readings visually reach a plateau phase. During the fourth phase (P4) the is an ongoing temperature increase until it stabilizes. The values of moisture sensor do not change significantly since the temperature dependency at dry state is minimal.

There are several advantages of simply using temperature sensor data for determining the $\Delta\theta_x$. First, moisture sensor data or moisture measurements is always a volume average. Hence, moisture profile as shown in Fig. 12 does not precisely define the transition between dry and wet zones. Secondly, the accuracy of temperature sensor location can have a large impact on the temperature profiles (Fig. 13). This leads to inaccurate determination of the point where the slope of the temperature profile changes. Thirdly, if the dry out process is slow or the sample loses water over time due to evaporation, the temperature profile does not stabilize again leading to inaccurate determination of $\Delta\theta_x$. Using only temperature time series data provide a reasonable estimation of $\Delta\theta_x$ while at the same time eliminating all the above-mentioned problems. In other words, temperature data is nearly a point measurement, the accuracy of the sensor location is not relevant, and the test does not have to reach a steady state.

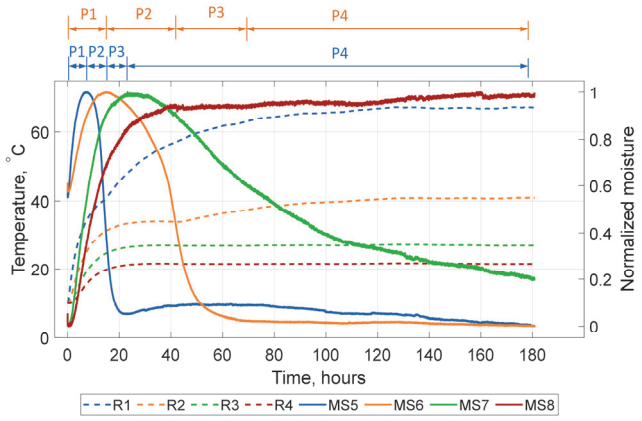

Fig. 14. Moisture and temperature sensor response in a test with dry zone formation. Duration of phases P1-P4 are indicated for the two positions closes to the heat source. R1-R4 are temperature and MS5-MS8 are moisture sensors normalized to max reading, horizontally away from the core.

Observation in Fig. 14 makes it clear that using temperature sensors to determine the progression of dry zone with the associated $\Delta\theta_x$ is sufficient. The moisture sensors could be used in combination with the temperature sensors to validate the dry-zone progression. However, the moisture sensor data is not necessary to determine the $\Delta\theta_x$. Fig. 15 shows temperature time series for REN material with different moisture contents: a) 3.2%, b) 2.4% and c) 1.6%. With decreasing moisture content, the size of the dry zone increases. With larger dry zone, more critical temperature points can be read from the experiment, by observing the break in the rising temperature curve. If the temperature rise is too rapid the exact point of critical temperature increase can be impossible to read. This can be seen in Fig. 15c with moisture content of 1.6%.

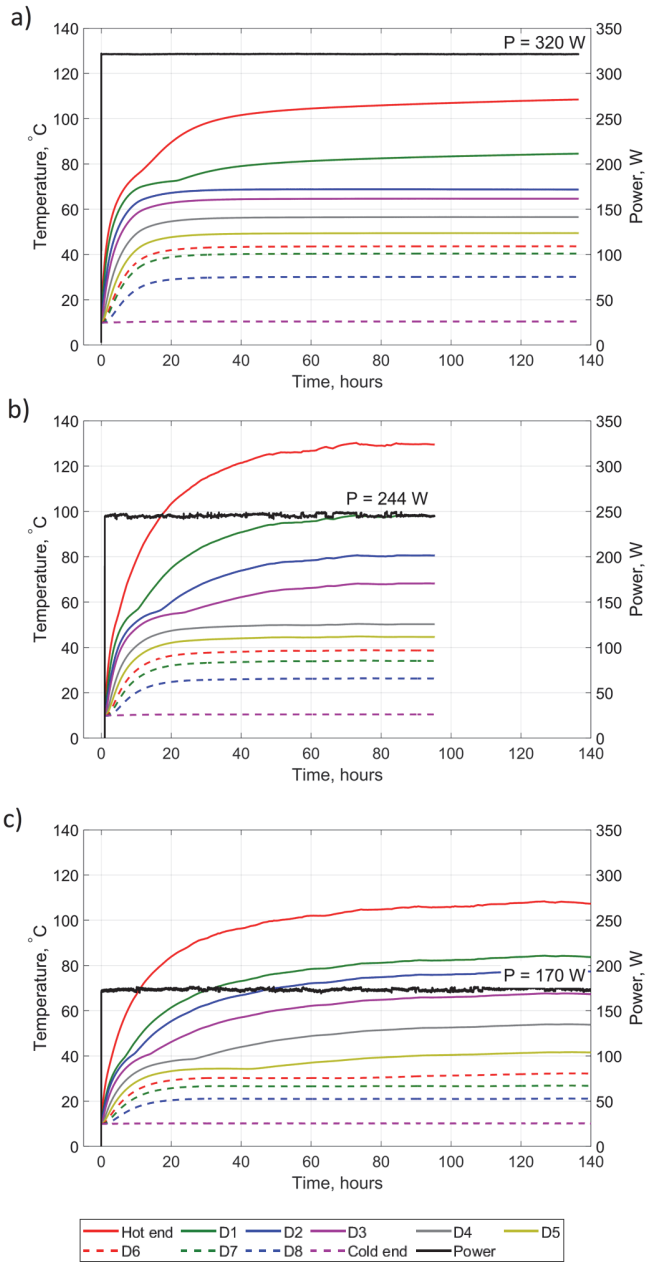

Fig. 15. Temperature time series for REN material with different moisture content: a) w=3.2%; b) w=2.4%; c) w=1.6%. Temperature sensor D1 is closest on underside of core, while D8 is furthest away on underside of core.

The temperature sensor placed directly on the heating element transitions into the dry phase so quickly that the deflection point is not visible. However, with moisture content of 1.6% the dry zone is large enough to have multiple measurements of critical temperature further away from the heating cable.

Fig. 16 summarizes measured values of $\Delta\theta_x$ from all experiments where dry-out zone formed, and values of $\Delta\theta_x$ averaged over distance from core is given in Table IV. There is a noticeable difference in terms of the performance. Generally, natural sand (NAT) has substantially lower $\Delta\theta_x$ compared to any of the two crushed rock sands (REN, VAS). The difference is increasing with increasing moisture content. At moisture content of 3.2% the $\Delta\theta_x$ varies from 45°C for natural sand (NAT) up to 73°C for crushed rock material (VAS). Comparing NAT and REN material, one can see that NAT sand with 3.2% of water has about the same value of $\Delta\theta_x$ as REN sand with 2.4% moisture content. This emphasizes the effect of material on the $\Delta\theta_x$ for the same moisture content. Given that porosity for all materials is very similar, this also corresponds to the same degree of saturation (S_a).

These results clearly show the dependency of $\Delta\theta_x$ on the moisture content. This is a factor that in some studies is not taken into account when characterizing materials for their critical temperature rise [18]. The results generally show higher $\Delta\theta_x$ for crushed rock sands compared to other studies. Gouda et al. reports values of $\Delta\theta_x$ from 34 to 42 °C for naturals soils in [8] and $\Delta\theta_x$ from 27 to 38 °C for natural and artificial soils in [9], while Oh and Tinjum [18] reports values from 3 to 26 °C. For natural sands (NAT) with $\Delta\theta_x$ from 21 to 45 °C, the results correlate well with [8], [9]. However, as mentioned, other studies have tested materials for a limited range of moisture contents. To be able to accurately compare the experimental results, the $\Delta\theta_x$ should be defined as a function of degree of saturation.

The overall results of crushed rock sand having higher $\Delta\theta_x$ can be partly explained by the other geotechnical experiments presented before. There is a clear difference between VAS and NAT sand. VAS material could retain higher moisture content under no temperature gradient and under applied suction conditions. In addition, the hydraulic conductivity was substantially lower for VAS. When comparing REN and NAT material, the reason for having a large difference of $\Delta\theta_x$ is not very clear. Most of the geotechnical experiments did not provide a clear difference apart from the hydraulic conductivity test. It could be that some of the measurements do not have a clear correlation with the $\Delta\theta_x$ or that a particular measurement does not accurately depict the differences. For instance, the soil water characteristic curve could be determined for a finer fraction of the material. Even though the results for REN and NAT showed to be very similar, the REN material is generally much finer and also the pore size is smaller as shown by hydraulic conductivity tests. Hence, this should contribute to a higher moisture content for a given suction applied.

In Fig. 16 the value of $\Delta\theta_x$ tends to decrease as the dry zone grows larger, while it is expected that $\Delta\theta_x$ is specific to a given soil and moisture content. This is especially pronounced with the tests with 1.6% of moisture where the size of dry zone was more than 8 cm from the heating element. This contradicts the fact that in a closed system, the water content increases in the wet zone as the dry zone gets larger. Hence, the $\Delta\theta_x$ should increase since it requires higher $\Delta\theta_x$ for higher moisture contents. The test result shows the opposite effect. A possible explanation is that the moisture profile is very gradual as was shown in Fig 11. This means that as the dry zone progresses, at a given point in time, the moisture distribution is not the same as the initial moisture content. Generally, the progressing dry zone is adjacent to a zone that has a moisture content substantially below the ambient moisture content. Hence, the measured $\Delta\theta_x$ further away from the heating element can be below the values that were measured when the moisture content was more evenly distributed.

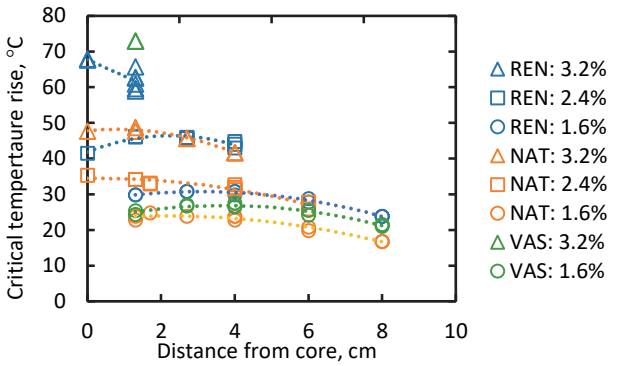

Fig. 16. The rise of critical temperature at different distance from heat source for three tested soils.

TABLE V
CRITICAL TEMPERATURE RISE FOR SOILS WITH DIFFERENT MOISTURE CONTENTS

Material	*Moisture content % dry weight*	*Saturation, S_r*	*$\Delta\theta_x=\theta_x-\theta_a$*
REN (Crushed)	3,2	0.17	63,7
	2,4	0.13	44,6
	1,6	0.09	28,4
NAT (Natural)	3,2	0.15	45,1
	2,4	0.11	31,9
	1,6	0.09	21,4
VAS (Crushed)	3,2	0.15	72,9
	1,6	0.09	24,8

V. DISCUSSION

Reference [17] gives a method for determining the critical temperature rise for natural and crushed sand materials. The method is based on experimental measurements that are required to determine the η value that describes the moisture distribution under a given temperature gradient. The method gives an equation that yields the relationship between critical temperature rise and ambient degree of saturation and is given as:

$$\theta_{cr}-\theta_a=\frac{1}{\eta}\left[(1-S_{cr})^2\cdot\ln\frac{(1-S_{cr})}{(1-S_a)}-\frac{1}{2}(S_a^2-S_{cr}^2)-(S_a-S_{cr})\ (1-2\cdot S_{cr})\right] \quad (2)$$

where S_{cr} is critical degree of saturation and S_a is the ambient degree of saturation. Plotting the relationship for the two materials given by CIGRE [17] shows that there is a lower threshold for the ambient degree of saturation which refers to the critical degree of saturation (Fig. 17). For a given value of critical temperature rise, any saturation value to the left from the line would result in a dry-out zone. Experimental data shows that there are two significant discrepancies when compared to the data from CIGRE [17]. First, the measured range of critical temperature rise for both material is at a significantly higher moisture content compared to the experimental results in this

study. Second, the measured data shows that the $\Delta\theta_x$ - S_a relationship extends towards the origin. This means that there is not a critical degree of saturation below which even a minor temperature gradient would cause a dry-out process. The critical degree of saturation following the method by CIGRE [17] for materials tested in this study is in the range from 0.31-0.40. These materials were tested at moisture contents that are substantially below their critical values, yet relatively high critical temperature rise was measured. This tends to show that even a low amount of moisture would require a certain temperature gradient to induce a dry-out process. Fig. 17 also shows experimental data from Oh and Tinjum [18] where several different materials were tested at a moisture content of 3%. The values are rather cluttered in a narrow range of $\Delta\theta_x$ since only one moisture content was tested. Nevertheless, these values are also significantly lower than the relationship given by CIGRE [17] and they also point to an ambient degree of saturation that is substantially lower than the critical value.

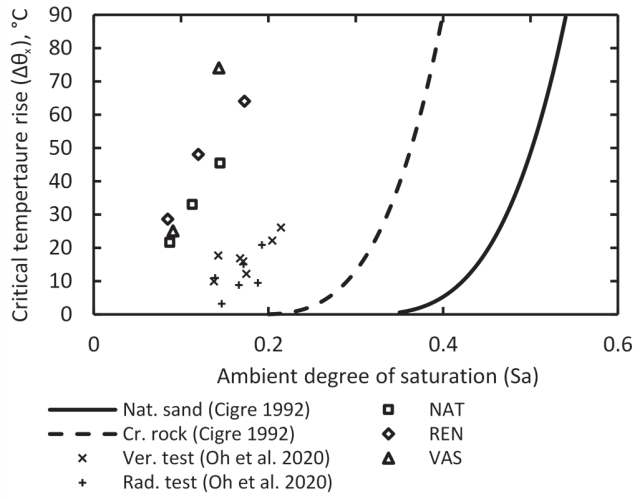

Fig. 17. The rise of critical temperature at different distance from heat source for three tested soils.

To quantify the effect of $\Delta\theta_x$ on ampacity, the formulae in IEC 60287 [11], [12], including dry-zone formation, was applied to a single core 132 kV XLPE cable, with parameters and laying geometry given in Appendix B. Experimental values of thermal resistivity was used for wet soils (Table III), while dry resistivity was calculated using the method on Côté and Konrad, given in Appendix A. The resulting ampacity as a function of critical temperature rise is given in Fig. 18, while the calculated ampacities for the measured moisture contents of all soils are given in Table V. For moisture contents of 1.6% and 2.4% natural sand (NAT) has the highest ampacity, while at moisture content of 3.2% VAS has the highest ampacity. Although having higher critical temperature rise is more favorable since it ensures relatively smaller dry zone around the cable, its effect on ampacity is not always predominant. The resulting ampacity is a combination of the thermal resistivity of materials and critical temperature rise. For a given material, critical temperature rise determines the size of the dry zone which subsequently has an influence on the overall thermal resistance of the soil. Given that all tested materials have roughly the same porosity, the thermal resistivity is governed by particle/mineral thermal conductivity. In this case the high quartz content of the natural sand (NAT) yielded a lower thermal resistivity in the dry state compared to the crushed rock sands (REN, VAS). The effect of thermal resistivity at higher moisture content becomes less predominant. Instead, having higher critical temperature rise can ensure higher ampacity. This means that when selecting a cable sand, it should not selected be solely based on critical temperature rise. Instead, ampacity should be calculated, to ensure that the effect of both, thermal resistivity, and critical temperature rise, is considered.

For cable installations in arid areas, where expected ambient moisture content is low, the application of a natural sand with high quartz content would be beneficial, even when dry soil is assumed, compared to crushed rock sand with a low moisture content. If seepage and precipitation will provide a high ambient moisture level throughout the year, a crushed rock soil would be beneficial, although the particle distribution should be considered. A high amount of fines provides a higher critical temperature rise, but could have negative effects on the mechanical properties over time in terms of cementation [10].

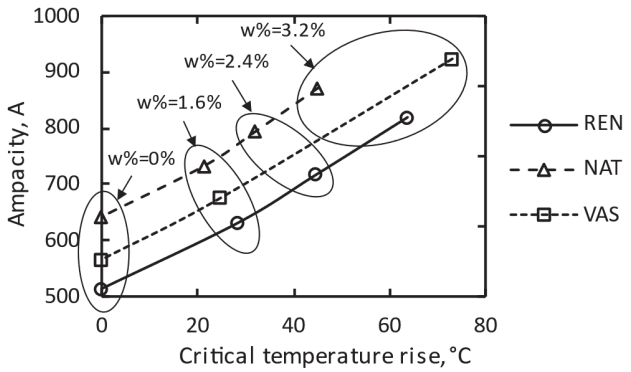

Fig. 18. Calculated ampacity values based on experimental results.

TABLE VI
CALCULATED AMPACITY VALUES FOR SOILS WITH VARYING MOISTURE CONTENT CONSIDERING A DRY ZONE AROUND CABLES

Material	Moisture content (% dry weight)			
	0%	1.6%	2.4%	3.2%
	I (A)	I (A)	I (A)	I (A)
REN	515	633	719	821
NAT	644	734	794	872
VAS	565	676	-	925

VII. CONCLUSION

This study experimentally investigated dry-out process for three commonly used backfill soils for power cable installations. Materials were tested in a cylindrical test cell with a cylindrical heating element in the centre of the cell. The samples were tested with moisture contents 1.6 %, 2.4% and 3.2% of dry weight, and constant power for each of the moisture contents, 170, 240 and 320 W, respectively.

Time series of temperature sensor data were used to determine the critical temperature rise ($\Delta\theta_x$). Values of $\Delta\theta_x$ ranged from 21 to 45 °C for natural soil and 25 to 73 °C for crushed rock soils, depending on moisture content. Generally, natural sand dries out at significantly lower temperatures at all ambient moisture levels compared to crushed rock. Multiple geotechnical experiments were carried out to indicate the characteristic that makes the difference between the materials

in terms of the $\Delta\theta_x$. The amount of fines and the SWCC are the two characteristics that provide partial explanation. However, one of the crushed rock sands and natural sand has very similar characteristics, yet they have a very different $\Delta\theta_x$. This could be partly attributed to the fact that, even though the REN sand has a low amount of fines, the average particle size is much smaller.

Ampacity was calculated for a 132 kV XLPE cable using experimentally measured values of $\Delta\theta_x$. The results show that at low moisture content, low thermal resistivity can compensate for a low $\Delta\theta_x$. This is the case for natural sand having lower $\Delta\theta_x$ compared to crushed rock materials yet yielding higher ampacity at low moisture content. In contrary, at relatively high moisture content, $\Delta\theta_x$ becomes more predominant governing the overall ampacity. The values for thermal resistivity and critical temperature increase presented are representative for commonly applied backfill materials and should thus provide more accurate ampacity calculations under similar conditions of ambient moisture.

APPENDIX

Appendix A: Method for estimating thermal resistivity

Côté and Konrad have published a model for estimating thermal conductivity over a broad range of natural and crushed soils, based on the normalized conductivity approach [5], [24].

The normalized thermal conductivity λ_r is defined as:

$$\lambda_r = \frac{\lambda - \lambda_{dry}}{\lambda_{sat} - \lambda_{dry}}, \tag{3}$$

where λ is the actual thermal conductivity and λ_{dry} and λ_{sat} the thermal conductivities in dry and saturated states, respectively. The modelled relative thermal conductivity can be expressed as

$$\lambda_r = \frac{\kappa \cdot S_r}{1 + (\kappa - 1) \cdot S_r}, \tag{4}$$

where κ is an empirical parameter describing different soils. For unfrozen natural and crushed rock sands κ is 3.6 and 4.5, respectively. S_r is the degree of saturation and is calculated as:

$$S_r = \frac{w}{100} \frac{\rho_d}{n \cdot \rho_w}, \tag{5}$$

where w is water content, ρ_d dry density, ρ_w density of water, and n is the porosity, which is expressed as

$$n = 1 - \frac{\rho_d}{\rho_s}, \tag{6}$$

where ρ_s is the density of solid particles. The saturated thermal conductivity is estimated by the geometric mean:

$$\lambda_{sat} = \lambda_s^{1-n} \cdot \lambda_w^n, \tag{7}$$

where λ_s and λ_w are particle and water thermal conductivity, respectively. Dry thermal conductivity is calculated as

$$\lambda_{dry} = \frac{(k_{2p} \cdot \lambda_s - \lambda_f)(1-n) + \lambda_f}{1 + (k_{2p} - 1)(1-n)}, \tag{8}$$

where λ_f is the thermal conductivity of air and k_{2p} is a structure parameter given by

$$k_{2p} = 0.29 \left(15 \frac{\lambda_f}{\lambda_s}\right)^{\beta}, \tag{9}$$

where β is an empirical structure parameter. For $\lambda_f/\lambda_s < 1/15$, β is 0.81 and 0.54 for natural and crushed rock soils, respectively. Finally, the thermal resistivity *TR* is calculated as the inverse of thermal conductivity

$$TR = \frac{1}{\lambda}. \tag{10}$$

Appendix B: Cable parameters and assumptions

The modelled cable in this work was a 132 kV XLPE insulated high voltage cable with 630 mm^2 Cu cross-section and 170 mm^2 Al screen. The geometry of the cable is shown in Fig. 19, while relevant parameters for cable in Table VI and Cable installation details in Table VII. Ampacity calculations were performed by implementing IEC 60287 [11], [12] in Python code.

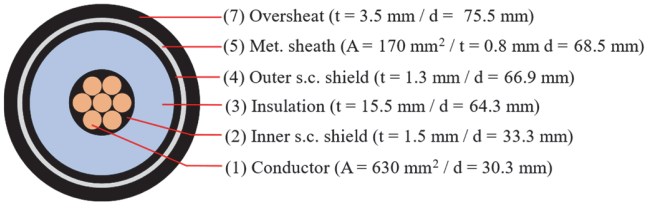

Fig. 19. Construction of cable used in this work. The number of strands is not correct and for illustration purposes only.

TABLE VII
MATERIAL PARAMETERS FOR CABLE. TR IS THERMAL RESISTIVITY.

Layer	Material	Property
Conductor	Cu, stranded	R_{DC} = 0.0283 Ω/km at 20 °C
Insulation	XLPE	TR = 3.5 K.m/W
Screen	Al, welded	R_{DC} = 0.167 Ω/km at 20 °C
Oversheath	HDPE	TR = 3.5 K.m/W

TABLE VIII
CABLE INSTALLATION DETAILS

Parameter	Value
Laying depth	1000 mm
Ambient temperature	20 °C
Configuration	Trefoil
Screen	Connected in both ends
Voltage	132 kV

ACKNOWLEDGMENTS

This work was supported in part by the Norwegian Research Council under Grant 296215. Henrik Strand, SINTEF Energy Research is acknowledged for contributing to IEC 60287 scripts.

REFERENCES

[1] Cigré, "The conditions controlling the drying-out of soil around power cables," *Electra*, vol. 84, 1982.

[2] Cigré, "Current ratings of cables buried in partially dried out soil. Part 1: Simplified method that can be used with minimal soil information: 100(% load factor)," *Electra*, vol. 104, pp. 11–22, 1986.

[3] O. T. Farouki, "Thermal Properties of Soils," COLD REGIONS RESEARCH AND ENGINEERING LAB HANOVER NH, Dec. 1981. Accessed: Jun. 09, 2022. [Online]. Available: https://apps.dtic.mil/sti/citations/ADA111734

[4] O. Johansen, "Thermal Conductivity of Soils," COLD REGIONS RESEARCH AND ENGINEERING LAB HANOVER NH, 1977.

Accessed: May 04, 2022. [Online]. Available: https://apps.dtic.mil/sti/citations/ADA044002

[5] J. Côté and J.-M. Konrad, "A generalized thermal conductivity model for soils and construction materials," *Can. Geotech. J.*, vol. 42, no. 2, pp. 443–458, Apr. 2005, doi: 10.1139/t04-106.

[6] E. C. Rusty Bascom, N. Patel, and D. Parmar, "Thermal environment design considerations for ampacity of buried power cables," in *2014 IEEE PES T&D Conference and Exposition*, Chicago, IL, USA, Apr. 2014, pp. 1–5. doi: 10.1109/TDC.2014.6863561.

[7] F. de Leon and G. J. Anders, "Effects of backfilling on cable ampacity analyzed with the finite element method," *IEEE Transactions on Power Delivery*, vol. 23, no. 2. pp. 537–543, 2008.

[8] O. E. Gouda, A. Z. El Dein, and G. M. Amer, "Effect of the formation of the dry zone around underground power cables on their ratings," *IEEE Transactions on Power Delivery*, vol. 26, no. 2, pp. 972–978, Apr. 2011, doi: 10.1109/TPWRD.2010.2060369.

[9] O. E. Gouda and A. Z. El Dein, "Improving underground power distribution capacity using artificial backfill materials," *IET Generation, Transmission & Distribution*, vol. 9, no. 15, pp. 2180–2187, Nov. 2015, doi: 10.1049/iet-gtd.2015.0274.

[10] E. C. Bascom, A. E. Shirer, and D. E. Anderson, "Impact of Cementation and Burial Depth on Soil Thermal Properties Used for Power Cable Design in Arid Climates," in *2022 IEEE/PES Transmission and Distribution Conference and Exposition (T&D)*, Apr. 2022, pp. 01–05. doi: 10.1109/TD43745.2022.9816881.

[11] International Electrotechnical Commision, "IEC 60287 Electric cables - Calculation of the current rating - Part 1-1: Current rating equations (100 % load factor) and calculation of losses - General," 2006.

[12] International Electrotechnical Commision, "IEC 60287 Electric cables - Calculation of the current rating - Part 2-1: Thermal resistance - Calculation of thermal resistance," 2015.

[13] F. Donazzi, E. Occhini, and A. Seppi, "Soil thermal and hydrological characteristics in designing underground cables," *Proceedings of the Institution of Electrical Engineers*, vol. 126. IET, pp. 506–516, 1979.

[14] J. I. Adams, "The thermal behavior of cable backfill materials," *IEEE Transactions on Power Apparatus and Systems*, vol. PAS-87, no. 4, pp. 1149–1161, Apr. 1968, doi: 10.1109/TPAS.1968.292094.

[15] W. Hadley and R. Eisenstadt, "A critical soil moisture condition affecting buried transmission cables [includes discussion]," *Transactions of the American Institute of Electrical Engineers. Part III: Power Apparatus and Systems*, vol. 72, no. 5. pp. 849–854, 1953.

[16] H. Radhakrishna, F. Chu, and S. Boggs, "Thermal stability and its prediction in cable backfill soils," *IEEE transactions on power apparatus and systems*, no. 3. pp. 856–867, 1980.

[17] Cigré, "Determination of a value of critical temperature rise for a cable backfill material," *Electra*, vol. 145. pp. 15–29, 1992.

[18] H. Oh and J. M. Tinjum, "Comparison of two laboratory methods for measuring soil critical temperature," *Geotechnical Testing Journal*, vol. 44, no. 2, pp. 339–357, 2020.

[19] O. E.-S. Gouda, G. F. A. Osman, W. A. A. Salem, and S. H. Arafa, "Cyclic Loading of Underground Cables Including the Variations of Backfill Soil Thermal Resistivity and Specific Heat With Temperature Variation," *IEEE Transactions on Power Delivery*, vol. 33, no. 6, pp. 3122–3129, Dec. 2018, doi: 10.1109/TPWRD.2018.2849017.

[20] H. Lu, F. De Leon, D. N. Soni, and W. Wang, "Two-zone geological soil moisture migration model for cable thermal rating," *IEEE Transactions on Power Delivery*, vol. 33, no. 6. pp. 3196–3204, 2018.

[21] P. Ocłoń, P. Cisek, M. Pilarczyk, and D. Taler, "Numerical simulation of heat dissipation processes in underground power cable system situated in thermal backfill and buried in a multilayered soil," *Energy Conversion and Management*, vol. 95. pp. 352–370, 2015.

[22] EN 1097-7:2008, "Tests for mechanical and physical properties of aggregates - Part 7: Determination of the particle density of filler - Pyknometer method," 2008.

[23] EN 933-1:2012, "Tests for geometrical properties of aggregates - Part 1: Determination of particle size distribution - Sieving method," 2012.

[24] EN 13286-2, "Unbound and hydraulically bound mixtures - Part 2: Test methods for laboratory reference density and water content - Proctor compaction".

[25] K. Rieksts, I. Hoff, E. Kuznetsova, and J. Côté, "Laboratory investigations of thermal properties of crushed rock materials," presented at the Tenth International Conference on the Bearing Capacity of Roads, Railways and Airfields, Athens, Greece, 2017.

[26] J. Côté and J.-M. Konrad, "Thermal conductivity of base-course materials," *Can. Geotech. J.*, vol. 42, no. 1, pp. 61–78, Feb. 2005, doi: 10.1139/t04-081.

[27] J. Côté and J.-M. Konrad, "Indirect methods to assess the solid particle thermal conductivity of Quebec marine clays," *Canadian geotechnical journal*, vol. 44, no. 9, pp. 1117–1127, 2007.

[28] METER group, "KSAT operation manual," 2022. [Online]. Available: http://manuals.decagon.com/Manuals/UMS/KSAT_Manual.pdf

[29] METER group, "HYPROP 2 operation manual," 2022. [Online]. Available: http://library.metergroup.com/Manuals/18263_HYPROP_Manual_Web.pdf

[30] G. P. Wind, "Capillary conductivity data estimated by a simple method," *Water in the Unsaturated Zone: Proc. UNESCO/IASH Symp., Wageningen, the Netherlands.*, pp. 181–191, 1968.

[31] U. Schindler, "Ein Schnellverfahren zur Messung der Wasserleitfähigkeit im teilgesättigten Boden an Stechzylinderproben," *Arch. Acker- u. Pflanzenbau u. Bodenkd*, vol. 24, pp. 1–7, 1980.

[32] D. G. Fredlund, A. Xing, and S. Huang, "Predicting the permeability function for unsaturated soils using the soil-water characteristic curve," *Canadian Geotechnical Journal*, vol. 31, no. 4. pp. 533–546, 1994.

[33] C. Balzer, C. Drefke, I. Sass, and K. Hentschel, "Enhanced adoption of the two-zone model to implement the drying out of soil in ampacity calculations of directly buried cable systems for different types of soil," *JICABLE'19 - 10th International Conference on Power Insulated Cables*. 2019.

[34] C. Drefke, M. Schedel, C. Balzer, I. Sass, V. Hinrichsen, and K. Hentchel, "Experimentelle Bestimmung der Dynamik von Bodenaustrocknung und der Wiederherstellung der Bodenfeuchte im Verteilnetz." 2016.

[35] T. Sakaki, A. Limsuwat, K. M. Smits, and T. H. Illangasekare, "Empirical two-point α-mixing model for calibrating the ECH2O EC-5 soil moisture sensor in sands," *Water resources research*, vol. 44, no. 4. 2008.

[36] F. Kizito *et al.*, "Frequency, electrical conductivity and temperature analysis of a low-cost capacitance soil moisture sensor," *Journal of Hydrology*, vol. 352, no. 3, pp. 367–378, May 2008, doi: 10.1016/j.jhydrol.2008.01.021.

[37] A. Moradi, K. M. Smits, J. Massey, A. Cihan, and J. McCartney, "Impact of coupled heat transfer and water flow on soil borehole thermal energy storage (SBTES) systems: Experimental and modeling investigation," *Geothermics*, vol. 57, pp. 56–72, Sep. 2015, doi: 10.1016/j.geothermics.2015.05.007.

BIOGRAPHIES

Karlis Rieksts received his M.Sc degree in 2015 from Riga Technical University (RTU) and his Ph.D degree in 2018 from Norwegian University of Science and Technology (NTNU). He currectly holds a position as postdoctoral fellow at NTNU. His work focuses on heat and mass trasfer in soils and construction materials. His been involved in projects related to frost protection for roads and railways, as well as moisture migration around buried power cables.

Espen Eberg received his M.Sc and Ph.D degrees in 2007 and 2011, respectively, from the Norwegian University of Science and Technology (NTNU) in Trondheim. His work focused on nanofabrication and transmission electron microscopy studies of ferroelectric materials and structures. Currently he holds a position as research scientist at SINTEF Energy Research where he conducts R&D projects focusing on condition assessment of electric power apparatus and ampacity calculations. He is also the project manager for the Norwegian National Research Infrastructure ElpowerLab.